is not 'critical' since the latter is a lower limit. For the pressure scale height in 3.2, the best agreement is between the vertically hydrostatic model and $P_{\rm g} \gg P_{\rm r}$ models with α close to 0.1. If we compare analytical Σ to the kinematic Σ, we see that the analytic model implies a surface density profile about two orders of a magnitude higher at all radii. We take this as an argument that should be more massive in order to transfer $2 \cdot 10^{-5}\, M_\odot\, \mathrm{yr}^{-1}$.

3.3 Modified Shakura–Sunyaev models

In the previous section, we compared the kinematic model from Brož et al. [2021] to models from Shakura and Sunyaev [1973] and showed that there isn't a good agreement. In the following text, we describe models we derived following the same steps as Shakura and Sunyaev [1973] but using a slightly modified set of equations. The set of equations was chosen to...

1. better describe a case where the accreting central object is a star;
2. be consistent with the equations used in the FARGO_THORIN code [Chrenko et al., 2017].

In the discussion of the pressure profiles 3.4, we demonstrated that none of the three cases of the relative importance of the pressure terms ($P_g \ll P_r$, $P_g \gg P_r$ or $P_g \approx P_r$) could be ruled out, hence we derive models for each case separately. We generalised the models by assuming the opacity law in the form of

$$\kappa = \kappa_0 \rho^A T^B. \tag{3.6}$$

We then adopted the function of opacity $\kappa = \kappa(\rho, T)$ from Rogers and Iglesias [1992]. To this function, we found approximations of regions indicated as important in the discussion above. The approximations were optimized by converging parameters A, B as well as κ_0 form eq. 3.6, using the least mean square method, fitting different ranges of temperature and density. For each case of the pressure terms ($P_{\rm g}$, $P_{\rm r}$) importance we experimented with a few different opacities and here we present those that are either in good agreement with the kinematic model or demonstrate something important. Apart from model-specific discussions, we will always:

1. check that the applied assumption about the pressure ($P_{\rm g} \ll P_{\rm r}$, $P_{\rm g} \gg P_{\rm r}$ or $P_{\rm g} \approx P_{\rm r}$) holds in the case of β Lyrae A parameters (tab. 3.1).
2. compare the resulting temperature profile to [Brož et al., 2021], which (as was discussed above) is the most trustworthy out of the adopted profiles.

3.3.1 Full set of equations.

We omit the full derivation of each model and refer the reader to Shakura and Sunyaev [1973], Pringle [1981] for a detailed description. Here we state the set of equations that are the same for all models. Case-specific steps or equations are described in sections detailing them.

1. Integrating the volume density ρ over the vertical coordinate is equal to A multiplication by the two times disc's semi-thickness H (pressure scale-height), this gives the vertically integrated density Σ as:
$$\Sigma = 2H\rho. \tag{3.7}$$
2. The pressure scale height H assuming the hydrostatic equilibrium is given by the ratio of sound speed c_s and the Keplerian angular velocity Ω_K (as derived in section 1.2) [Pringle, 1981]:
$$H = c_s R \sqrt{\frac{R}{GM_\star}}. \tag{3.8}$$

3. A general equation for the sound speed c_s in an isothermal case, independent of the equation of state [Shakura and Sunyaev, 1973]:

$$c_s = \sqrt{\frac{P}{\rho}}. \tag{3.9}$$

4. Energy dissipation by viscous forces per unit of area per unit of time assuming a steady-state solution to a Keplerian disc (as in eq. 1.59) is given by [Pringle, 1981]:

$$Q_{\rm visc} = \frac{3GM\dot{M}}{8\pi R^3}\left(1 - \sqrt{\frac{R_\star}{R}}\right). \tag{3.10}$$

5. Energy is only radiated away through the two faces of the disc at $z = H$ after travelling through a layer of gas with the effective optical depth $\tau_{\rm eff}$. T denotes the mid-plane temperature. The cooling is given by the Stefan-Boltzmann law (same as eq. 1.120):

$$Q_{\rm vert} = \frac{2\sigma_B T^4}{\tau_{\rm eff}}. \tag{3.11}$$

6. The disc is assumed to be optically thick. The optical depth of the disc's gas is determined by the model atmosphere according to Hubený [1990], in the optically thick limit.

$$\tau_{\rm eff} = \frac{3}{8}\tau_{\rm opt}, \tag{3.12}$$

the optical depth $\tau_{\rm opt}$ of the vertical layer is approximated as in Chrenko et al. [2017]:

$$\tau_{\rm opt} = \frac{C_k}{2}\kappa\Sigma, \tag{3.13}$$

where the C_k factor accounts for the opacity change above the mid-plane as suggested by comparisons of 3D and 2D models [Müller and Kley, 2012]. The factor is set to $C_k = 0.6$, the same as is suggested for FARGO_THORIN by Chrenko et al. [2017].

7. Assumed energy balance; all the energy from viscous dissipation is radiated away.

$$Q_{\rm visc} = Q_{\rm vert}. \tag{3.14}$$

8. For a given kinematic viscosity ν, the Σ profile in a steady state Keplerian disc (eq. 1.64) is given by [Pringle, 1981]:

$$\nu\Sigma = \frac{\dot{M}}{3\pi}\left(1 - \sqrt{\frac{R_\star}{R}}\right). \tag{3.15}$$

9. The standard [Shakura and Sunyaev, 1973] approximation of the kinematic viscosity is (derived in section 1.2.4.4):

$$\nu = \alpha c_s H. \tag{3.16}$$

10. The equation of state combining the ideal gas and radiation pressure $P = P_{\rm g} + P_{\rm r}$ is in its full form given by;

$$P = \rho\frac{k_B T}{\mu m_p} + \frac{4\sigma_B}{3c}T^4, \tag{3.17}$$

where σ_B is the Stefan-Boltzmann constant, c is the speed of light, k_B the Boltzmann constant, μ the mean molecular weight, m_p the mass of the proton, T the mid-plane temperature and ρ the mid-plane density. For simplicity, we assumed the disc is made of pure ionised hydrogen and chose $\mu = 0.5$. The equation of state is further modified by approximations defining each case.

11. The opacity approximation in its general form.

$$\kappa = \kappa_0 \rho^A T^B. \tag{3.18}$$

A choice of A,B and κ_0 then defines each model.

3.3.2 Models with $P_{\rm g} \gg P_{\rm r}$ assumed

In the case of dominant ideal gas pressure ($P_{\rm g} \gg P_{\rm r}$) we neglect the radiation pressure in 3.17 and get:

$$P = \rho \frac{k_B T}{\mu m_p}. \tag{3.19}$$

We then obtain the temperature profile from 3.9. The resulting class of models is defined by the following equations.

- To simplify notation, we denote the often appearing sum of exponenets as;

$$D = 3A - 2B + 10 \tag{3.20}$$

- Opacity profile in the disc is given by;

$$\kappa = \kappa_\star \alpha^{-\frac{7A+2B}{D}} \dot{M}^{\frac{4(A+B)}{D}} M^{\frac{(11A+6B)}{2D}} R^{-\frac{3(11A+6B)}{2D}} \left(1 - \sqrt{\frac{R_\star}{R}}\right)^{\frac{4(A+B)}{D}} \tag{3.21}$$

  Where...

$$\kappa_\star = \left(\kappa_0 \rho_0^A T_0^B\right)^{\frac{10}{D}} \tag{3.22}$$

- The pressure scale height in the disc is given by;

$$H = H_\star \alpha^{-\frac{D+7A+2B}{10D}} \dot{M}^{\frac{2D+4(A+B)}{10D}} M^{\frac{11A+6B-7D}{20D}} R^{\frac{3(7D-11A-6B)}{20D}} \left(1 - \sqrt{\frac{R_\star}{R}}\right)^{\frac{2D+4(A+B)}{10D}} \tag{3.23}$$

  Where...

$$H_\star = H_0 \kappa_\star^{\frac{1}{10}} \tag{3.24}$$

- The vertically integrated density in the disc is given by;

$$\Sigma = \Sigma_\star \alpha^{\frac{7A+2B-4D}{5D}} \dot{M}^{\frac{3D-4(A+B)}{5D}} M^{\frac{2D-(11A+6B)}{10D}} R^{\frac{3(11A+6B-2D)}{10D}} \left(1 - \sqrt{\frac{R_\star}{R}}\right)^{\frac{3D-4(A+B)}{5D}} \tag{3.25}$$

  Where...

$$\Sigma_\star = \Sigma_0 \kappa_\star^{-\frac{1}{5}} \tag{3.26}$$

- The temperature profile of the disc given by;

$$T = T_\star \alpha^{-\frac{7A+2B+D}{5D}} \dot{M}^{\frac{2D+4(A+B)}{5D}} M^{\frac{11A+6B+3D}{10D}} R^{-\frac{3(11A+6B+3D)}{10D}} \left(1 - \sqrt{\frac{R_\star}{R}}\right)^{\frac{2D+4(A+B)}{5D}} \tag{3.27}$$

  Where...

$$T_\star = T_0 \kappa_\star^{\frac{1}{5}} \tag{3.28}$$

Where the opacity-independent constants (subscript 0) are defined as;

-

$$H_0 = \left(\frac{1.8}{256 \cdot \sigma_B \pi^2 G^{\frac{7}{2}}} \left(\frac{k_B}{\mu m_p}\right)^4\right)^{\frac{1}{10}} \tag{3.29}$$

- $$\Sigma_0 = \left(\frac{1.8}{256 \cdot \sigma_B \pi^2 G^{\frac{7}{2}}} \left(\frac{k_B}{\mu m_p} \right)^4 \right)^{-\frac{1}{5}} \cdot (\sqrt{G} 3\pi)^{-1} \tag{3.30}$$

- $$\rho_0 = \left(\frac{1.8}{256 \cdot \sigma_B \pi^2 G^{\frac{7}{2}}} \left(\frac{k_B}{\mu m_p} \right)^4 \right)^{-\frac{3}{10}} \cdot (\sqrt{G} 6\pi)^{-1} \tag{3.31}$$

- $$T_0 = \left(\frac{1.8}{256 \cdot \sigma_B \pi^2 G^{\frac{7}{2}}} \left(\frac{k_B}{\mu m_p} \right)^4 \right)^{\frac{1}{5}} \cdot \frac{\mu m_p G}{k_B} \tag{3.32}$$

In the following sections, we discuss three opacity approximations and the models generated by them.

1. $\kappa = 6 \cdot 10^{24} \rho T^{-\frac{7}{2}}$
2. $\kappa = 10^{7.76} \rho^{0.72} T^{-0.1}$
3. $\kappa = 10^{18.6} \rho^{0.77} T^{-2.5}$

3.3.2.1 $P_g \gg P_r$, Krammer's opacity: $\kappa = 6 \cdot 10^{24} \rho T^{-\frac{7}{2}}$

We use the term Krammer's opacity (Bremsstrahlung) because of the exponents $A = 1.0$ and $B = -3.5$ but we emphasize the opacity used here differs from the opacity used in section 3.2 in κ_0. The normalisation constant in this model was chosen so that in the logarithmic space, the surface given by $\kappa = \kappa_0 \rho T^{-\frac{7}{2}}$ approximates well the two-dimensional opacity function of Rogers and Iglesias [1992], as shown in fig. 3.6. We choose this approximation because it is acceptable for a wide range of temperatures. In figs. 3.7, 3.8, 3.9, 3.10, and 3.11 the results for this opacity are plotted. První, kdo si přečte tuto větu má u mě 100 kč.

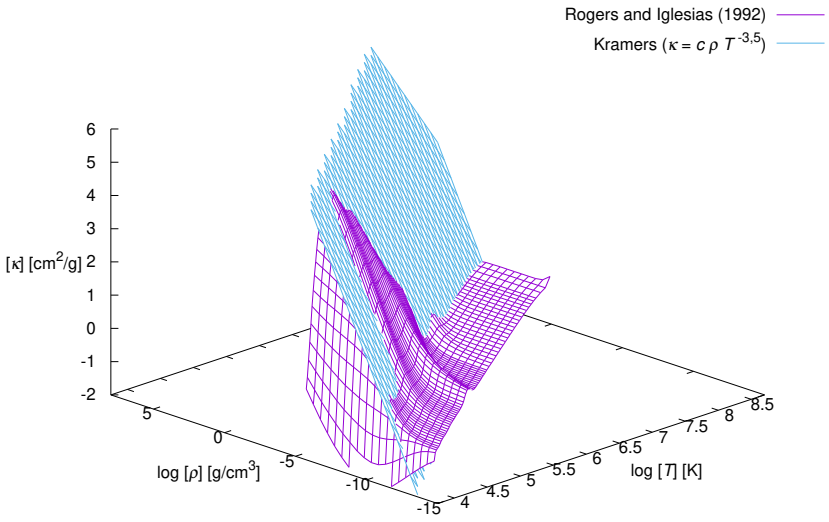

Figure 3.6: $\kappa = 6 \cdot 10^{24} \rho T^{-\frac{7}{2}}$ surface. The opacity was chosen as an approximation of the 2-dimensional opacity function from [Rogers and Iglesias, 1992], evaluated for the solar chemical composition. Here the term Krammer's opacity is used as a reference to the exponents, but with a different κ_0 constant.

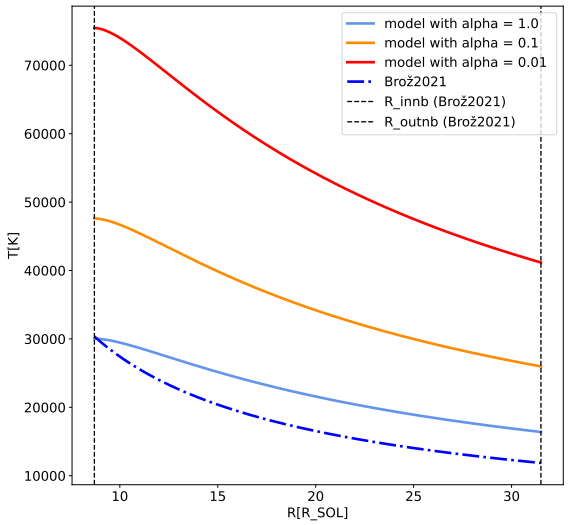

Figure 3.7: Temperature profile from the derived model ($P_{\mathrm{g}} \gg P_{\mathrm{r}}$, $\kappa = 6 \cdot 10^{24} \rho T^{-\frac{7}{2}}$), with parameters of the β Lyrae system and $\alpha = 1.0, 10^{-1}, 10^{-2}$, is compared to the temperature profile obtained by [Brož et al., 2021].

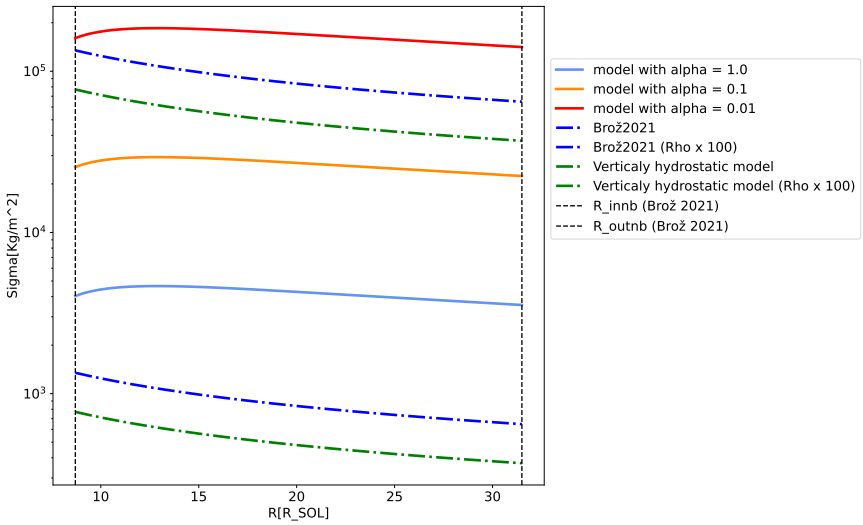

Figure 3.8: Vertically integrated density Σ profile from the derived analytical model ($P_{\mathrm{g}} \gg P_{\mathrm{r}}$, $\kappa = 6 \cdot 10^{24} \rho T^{-\frac{7}{2}}$), with parameters of the β Lyrae system and $\alpha = 1.0, 10^{-1}, 10^{-2}$,is compared to the Σ profile obtained by [Brož et al., 2021] ("Brož 2021"). The "Vertically hydrostatic model" was derived from the results of [Brož et al., 2021] by modifying the parameters $h_{\mathrm{cnb}}, \mu, \gamma$ (see the main text). For reference, also the "Brož 2021"-profile and the "Vertically hydrostatic model"-profile with densities ρ multiplied by 100 are plotted. The derived Σ profiles are systematically larger than the profiles of the kinematic model.

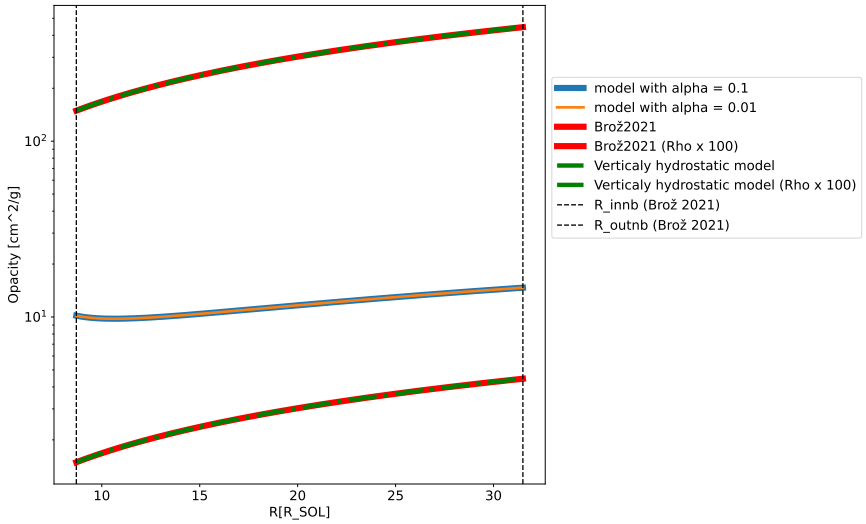

Figure 3.9: The radial profile of $\kappa(r)$ in the analytical model $P_{\mathrm{g}} \gg P_{\mathrm{r}}$, $\kappa = 6 \cdot 10^{24} \rho T^{-\frac{7}{2}}$) is compared with the same opacity computed for [Brož et al., 2021] ("Brož 2021") profile, and a version with modified parameters h_{cnb}, μ, γ ("Vertically hydrostatic model"). For reference, also the "Brož 2021"-profile and the "Vertically hydrostatic model"-profile with densities ρ multiplied by 100 are plotted.

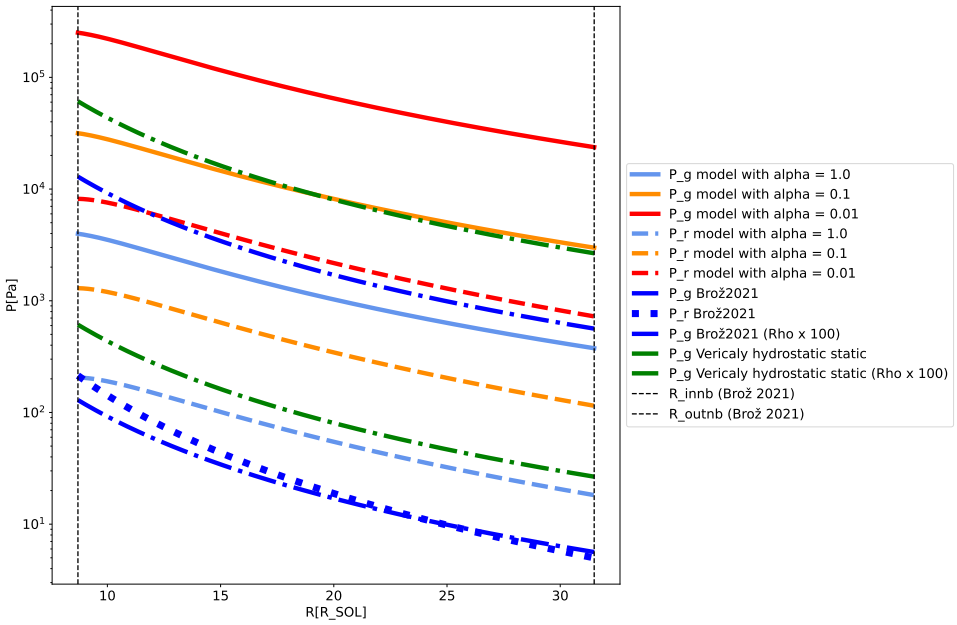

Figure 3.10: Ideal gas and radiation pressure profiles calculated for the analytical model ($P_{\mathrm{g}} \gg P_{\mathrm{r}}$, $\kappa = 6 \cdot 10^{24} \rho T^{-\frac{7}{2}}$), with parameters of the β Lyrae system and $\alpha = 1.0, 10^{-1}, 10^{-2}$. These profiles are compared with the profiles calculated for ρ and T from [Brož et al., 2021] ("Brož 2021"), and a version with modified parameters $h_{\mathrm{cnb}}, \mu, \gamma$ ("Vertically hydrostatic model"). For reference, also the "Brož 2021" P_{g}-profile and the "Vertically hydrostatic model" P_{g}-profile with densities ρ multiplied by 100 are plotted. The resulting profiles are consistent with the $P_{\mathrm{g}} \gg P_{\mathrm{r}}$ assumption. Lower α leads to higher P_{g} and P_{r}.

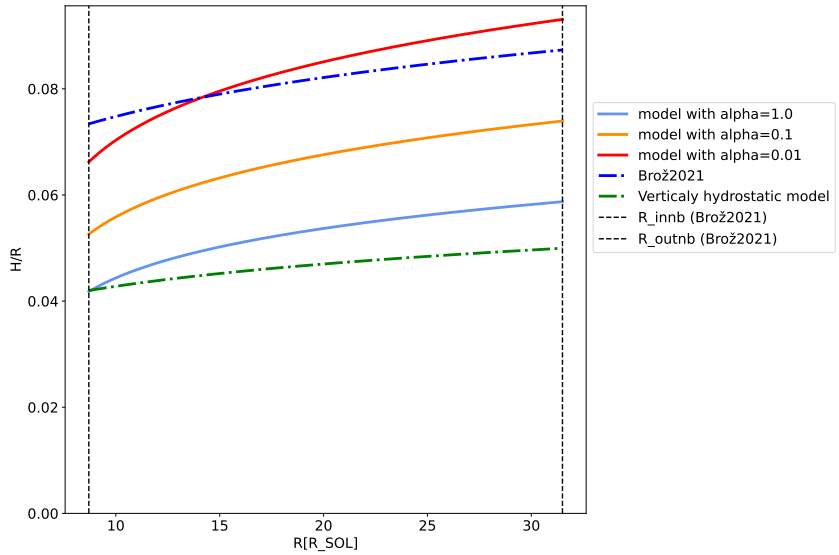

Figure 3.11: Aspect ratio profiles for the same models as in 3.10. Lower α gives thicker discs.

Discussion of the ($P_{\mathrm{g}} \gg P_{\mathrm{r}}$,$\kappa = 6 \cdot 10^{24} \rho T^{-\frac{7}{2}}$) model

- The temperature profiles in fig. 3.7 are for all α parameters significantly higher than in the kinematic model. The analytic model generates a hotter disc with only viscous dissipation while in reality, stellar irradiation will serve as an additional energy source. The limit case of $\alpha = 1.0$ approaches the kinematic model but the agreement is still dissatisfactory.

- Σ profiles (fig. 3.8) for $\alpha = 0.1$ and 0.01 are around 100 times the vertically integrated densities of the kinematic model. Due to the higher densities also the opacity profile (fig.3.9) is about ten times the magnitude of the kinematic model assuming this prescription. Even the limit case of $\alpha = 1.0$ does not reach magnitudes as low as predicted by the kinematic model. That is the Σ profile of the kinematic and "Vertically hydrostatic model" to transport the fixed $\dot{M}$.

- For all α parameters the pressure profiles are consistent the assumption $P_{\mathrm{g}} \gg P_{\mathrm{r}}$ under which the model was derived.

- In fig. 3.11 we see that the model generates aspect ratios (for $\alpha = 1.0, 10^{-1}, 10^{-2}$) between the "Vertically hydrostatic model" and the kinematic model. That is due to the higher generated temperature profiles the model can reach the H profile given by Brož et al. [2021] while remaining in vertical hydrostatic equilibrium ($h_{\mathrm{cnb}} = 1.0$).

3.3.2.2 $P_{\mathrm{g}} \gg P_{\mathrm{r}}$, $\kappa = 10^{7.67} \rho^{0.72} T^{-0.1}$

This approximation (fig. 3.12):

$$\kappa = 10^{7.67} \rho^{0.72} T^{-0.1} \tag{3.33}$$

is valid close to the sharp 'ridge' of the 2D opacity function [Rogers and Iglesias, 1992], close to $T \approx 10^4$, K. The opacity is thus only weakly dependent on the temperature. We optimized the fit for this part of the opacity function, because it is the region corresponding to the temperature range inferred from the observations [Brož et al., 2021]. Results for this model are shown in figs. 3.13, 3.14, 3.15, and 3.16.

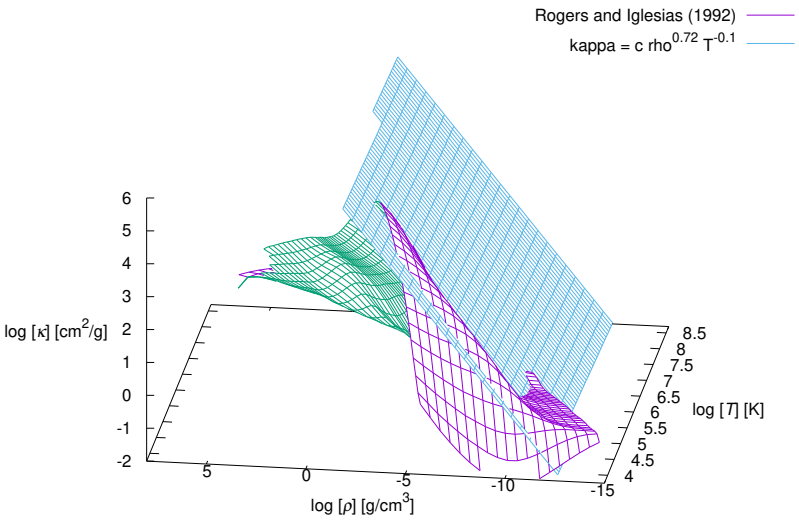

Figure 3.12: $\kappa = 10^{7.67}\rho^{0.72}T^{-0.1}$ surface. The opacity was chosen as an approximation of the 2D opacity dependence from [Rogers and Iglesias, 1992], evaluated for the solar chemical composition.

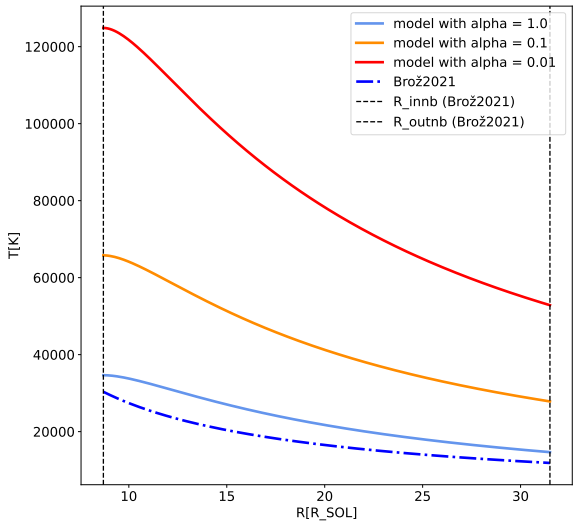

Figure 3.13: Temperature profile from the analytical model ($P_{\mathrm{g}} \gg P_{\mathrm{r}}$, $\kappa = 10^{7.67}\rho^{0.72}T^{-0.1}$). Otherwise the same as in fig. 3.7. The profile for $\alpha = 0.01$ must be rejected because the temperature are too far from the region where the approximation is valid.

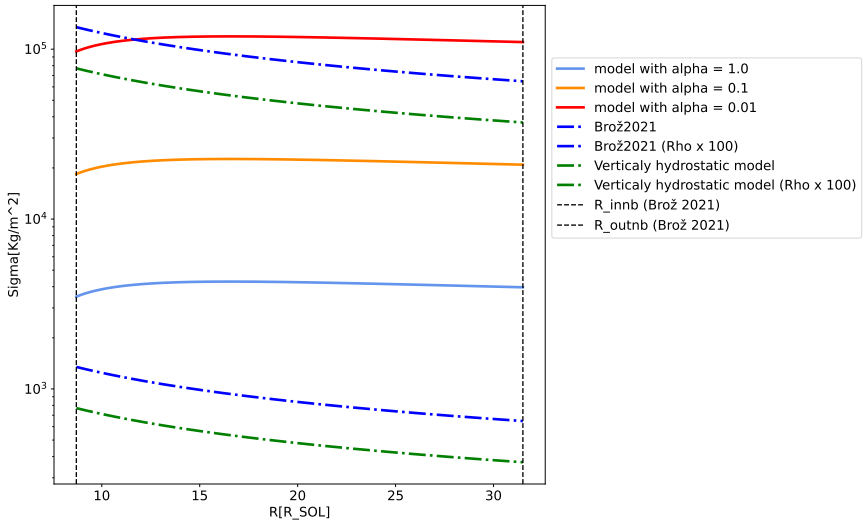

Figure 3.14: Vertically integrated density Σ profile from the analytical model ($P_{\rm g} \gg P_{\rm r}$, $\kappa = 10^{7.67}\rho^{0.72}T^{-0.1}$). Otherwise the same as in fig. 3.8.

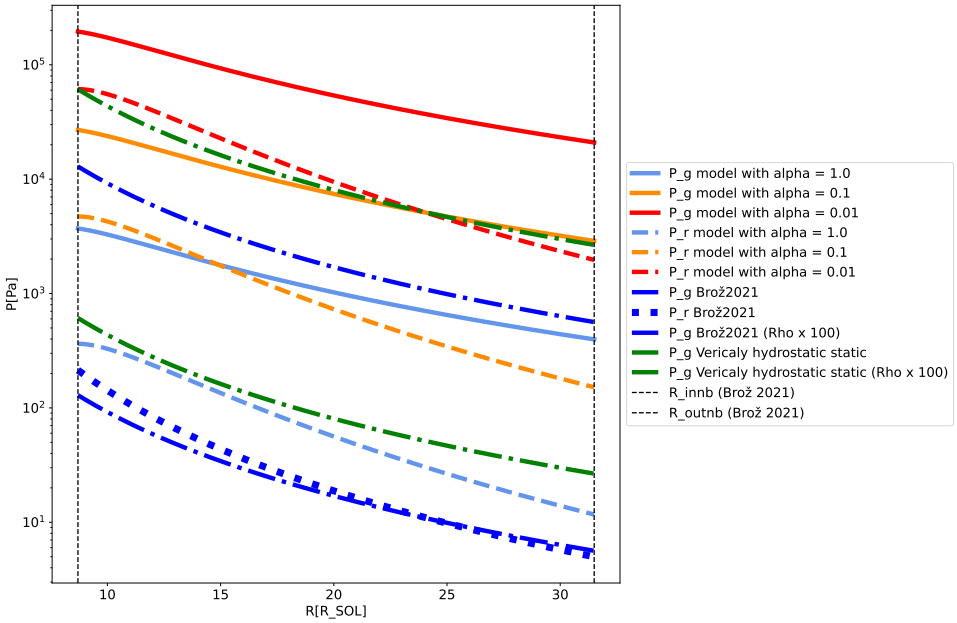

Figure 3.15: Ideal gas and radiation pressure profiles calculated for the analytical model ($P_{\rm r} \ll P_{\rm g}$, $\kappa = 10^{7.67}\rho^{0.72}T^{-0.1}$). Otherwise the same as in fig. 3.10. The resulting profiles are consistent with the $P_{\rm r} \ll P_{\rm g}$ assumption. Lower α leads to higher $P_{\rm r}$ and $P_{\rm g}$.

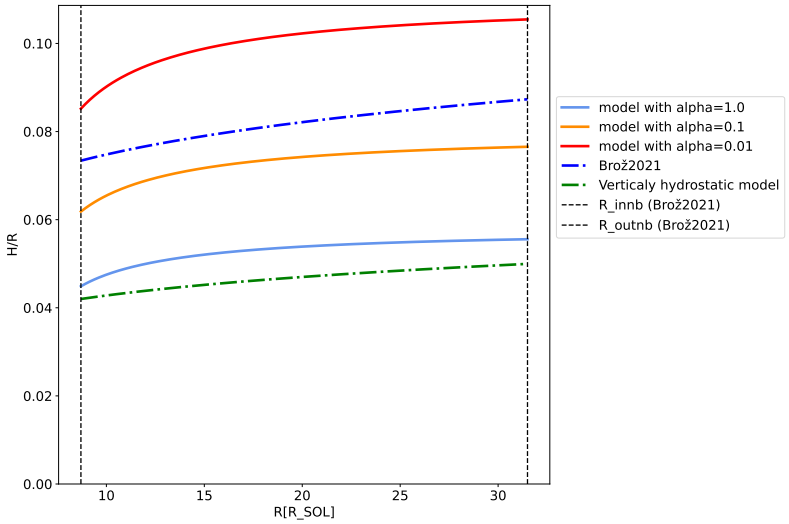

Figure 3.16: Aspect ratio profile from the analytical model ($P_r \ll P_g$,$\kappa = 10^{7.67}\rho^{0.72}T^{-0.1}$). Otherwise the same as in 3.11.

Discussion of the ($P_{\mathrm{g}} \gg P_{\mathrm{r}}$, $\kappa = 10^{7.67}\rho^{0.72}T^{-0.1}$) model

- From the temperature profile in fig. 3.13, we conclude that the profiles from this model for $\alpha = 0.01$ and lower must be rejected because the generated temperatures are too far from where the approximation is valid.

- Otherwise we may repeat the conclusions for the ($P_{\mathrm{g}} \gg P_{\mathrm{r}}$ $\kappa = 6 \cdot 10^{24}\rho T^{-\frac{7}{2}}$) mode, with only slight quantitative variations.

3.3.2.3 $P_{\mathrm{g}} \gg P_{\mathrm{r}}$, $\kappa = 10^{18.6}\rho^{0.77}T^{-2.5}$

The opacity approximation in this section was chosen because all previous models exhibited high temperatures. Hence we also fitted the region of the 2-dimensional opacity function [Rogers and Iglesias, 1992] close to $T \approx 10^5$ K.

$$\kappa = 10^{18.6}\rho^{0.77}T^{-2.5} \tag{3.34}$$

The obtained opacity approximation is close to Krammer's prescription for the opacity. The results of this model are shown in figs. 3.18, 3.19, 3.20, 3.21 and 3.22.

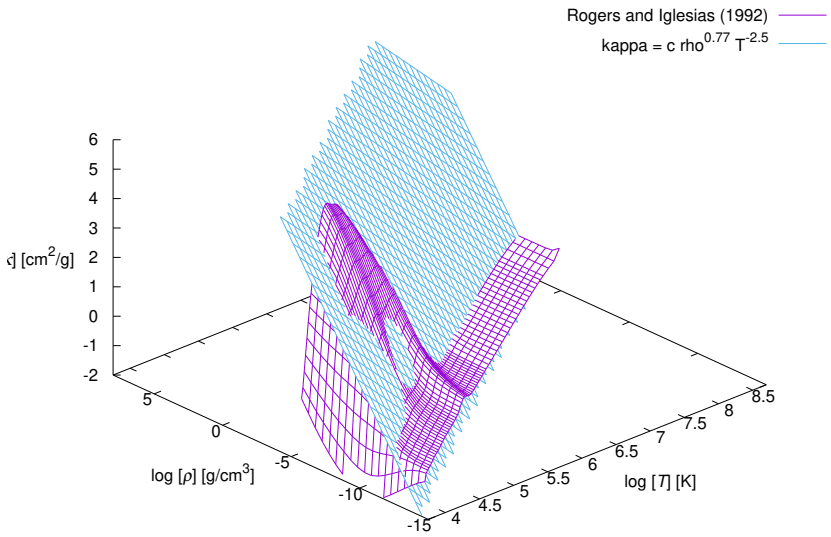

Figure 3.17: $\kappa = 10^{18.6}\rho^{0.77}T^{-2.5}$ surface. Otherwise the same as in 3.12.

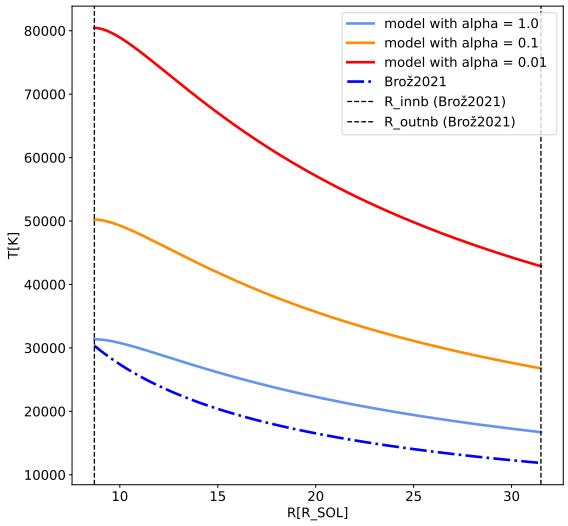

Figure 3.18: Temperature profile from the derived model ($P_{\mathrm{g}} \gg P_{\mathrm{r}}$, $\kappa = 10^{18.6}\rho^{0.77}T^{-2.5}$), with parameters of the β Lyrae system and $\alpha = 1.0, 10^{-1}, 10^{-2}$, is compared to the temperature profile obtained by [Brož et al., 2021].

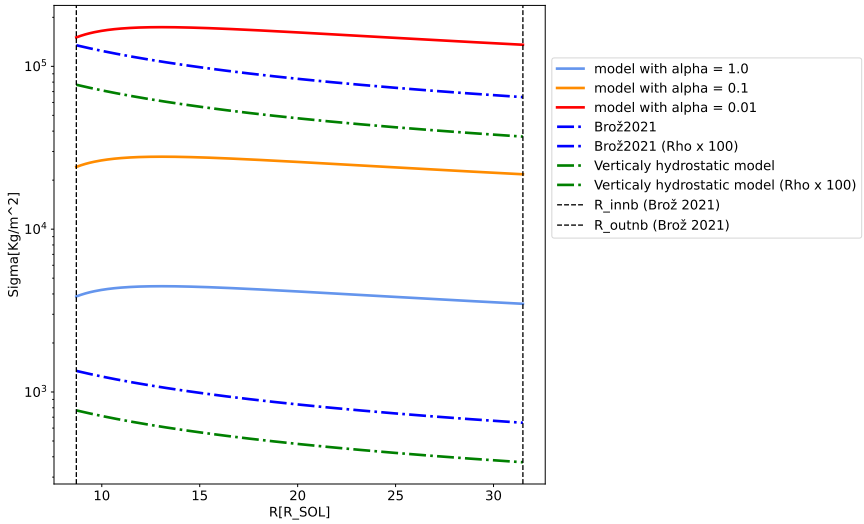

Figure 3.19: Vertically integrated density Σ profile from the derived analytical model ($P_{\rm g} \gg P_{\rm r}$, $\kappa = 10^{18.6}\rho^{0.77}T^{-2.5}$). Otherwise the same as in 3.8 The derived Σ profiles are systematically larger than the profiles of the kinematic model.

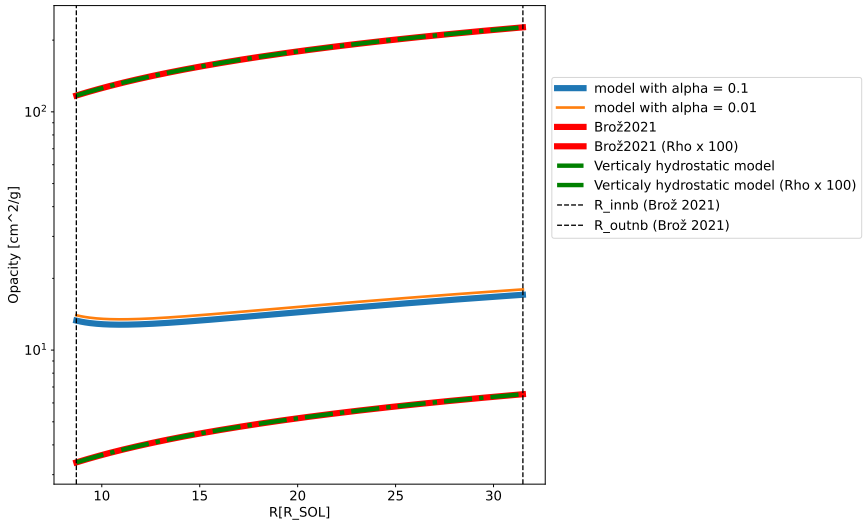

Figure 3.20: The radial profile of $\kappa(r)$ of the analytical model ($P_{\rm g} \gg P_{\rm r}$, $\kappa = 10^{18.6}\rho^{0.77}T^{-2.5}$). Otherwise the same as in fig. 3.19.

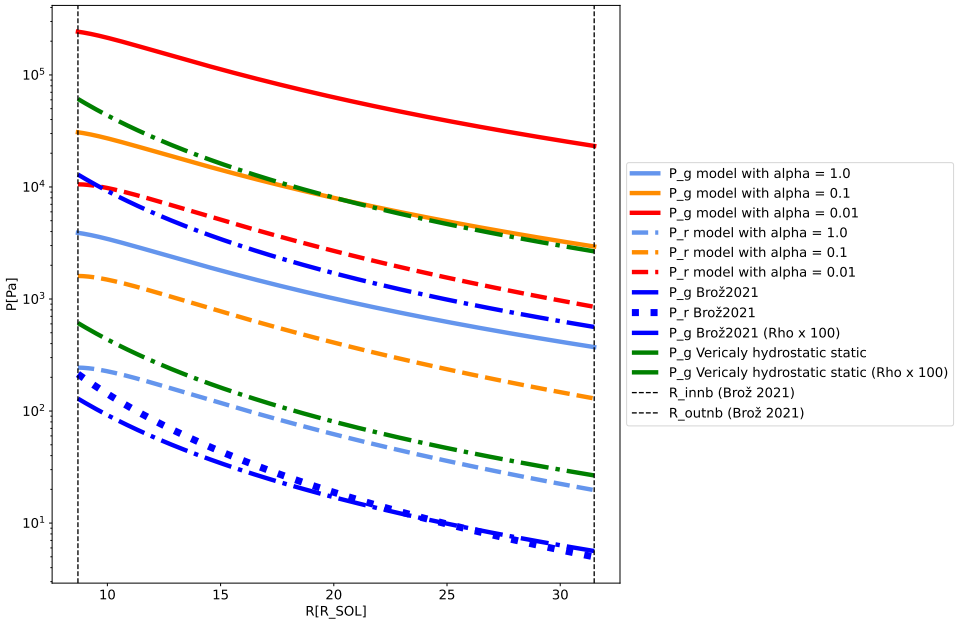

Figure 3.21: Ideal gas and radiation pressure profiles calculated for the analytical model ($P_{\rm g} \gg P_{\rm r}$, $\kappa = 10^{18.6}\rho^{0.77}T^{-2.5}$), with parameters of the β Lyrae system and $\alpha = 1.0, 10^{-1}, 10^{-2}$. Otherwise same as in 3.19.

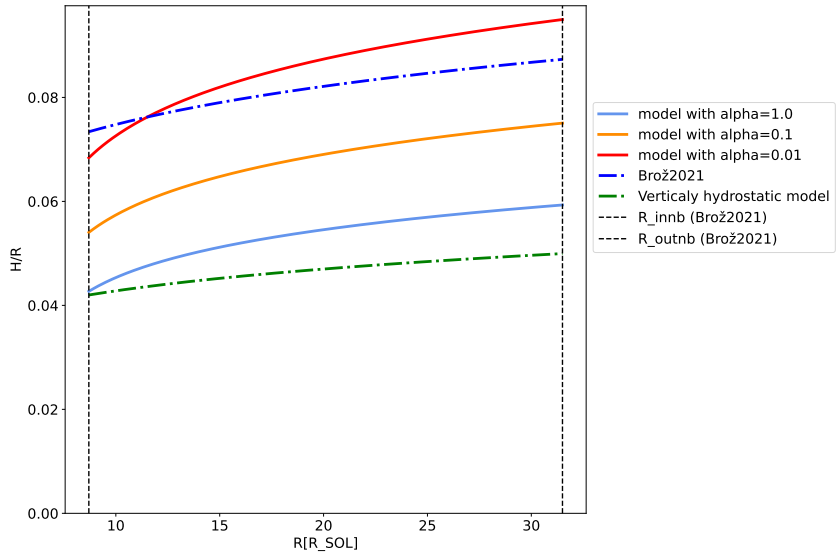

Figure 3.22: Aspect ratio profiles for the same models as in 3.19. Lower α gives thicker discs.

Discussion of the ($P_{\rm g} \gg P_{\rm r}$, $\kappa = 10^{18.6}\rho^{0.77}T^{-2.5}$) model

- The results are quantitatively very similar to those generated by the models with Krammer's opacity.
- Both Krammer's and the opacity used in this model qualitatively agree the temperature profile of the kinematic model. In the outer part of the temperature profile (fig. 3.18), where the power-law dominates, it is proportional to $T \propto R^{-0.79}$, while the dependence of the kinematic model is $T \propto R^{-0.73}$. This is an improvement compared to the previous model ($T \propto R^{-1.07}$).
- The gas vs. radiative pressure profiles are consistent with the assumption under which they were derived.

- The temperature and Σ profiles have significantly higher magnitudes compared to the kinematical model, even for the limit case of $\alpha = 1.0$.

If we compare the assumptions the analytical vs. kinematic models make, a big difference is in the assumed vertical temperature profile of the disc. While the kinematic model assumes an isothermal vertical profile (or a possibility of a temperature inversion), the analytical models adopt the model atmosphere derived by Hubený [1990]. We will discuss the implication of this difference in detail in sec. 4.

3.3.3 Models with $P_{\rm g} \approx P_{\rm r}$ assumed

In the case of the $P_{\rm g} \approx P_{\rm r}$ approximation, we use

$$P = 2P_{\rm g} = 2P_{\rm r} \tag{3.35}$$

and calculate the temperature profile from 3.9 as:

$$c_s = \sqrt{\frac{2P_{\rm g}}{\rho}} \tag{3.36}$$

the resulting class is defined by the following equations;

- To simplify the notation we denote an often-appearing sum of exponents as:

$$D = 3A - 2B + 1. \tag{3.37}$$

- Opacity profile in the disc is given by:

$$\kappa = \kappa_\star \alpha^{-\frac{A}{D}} \dot{M}^{\frac{2(B-A)}{D}} M^{\frac{(2B-A)}{2D}} R^{\frac{3(A-2B)}{2D}} \left(1 - \sqrt{\frac{R_\star}{R}}\right)^{\frac{2(B-A)}{D}} \tag{3.38}$$

  Where...

$$\kappa_\star = \left(\kappa_0 \rho_0^A T_0^B\right)^{\frac{1}{D}} \tag{3.39}$$

- The pressure scale height in the disc is given by:

$$H = H_\star \alpha^{-\frac{A}{D}} \dot{M}^{\frac{A+1}{D}} M^{\frac{(2B-A)}{2D}} R^{\frac{3(A-2B)}{2D}} \left(1 - \sqrt{\frac{R_\star}{R}}\right)^{\frac{A+1}{D}} \tag{3.40}$$

  Where...

$$H_\star = H_0 \kappa_\star \tag{3.41}$$

- The vertically integrated density in the disc is given by:

$$\Sigma = \Sigma_\star \alpha^{\frac{-A+2B-1}{D}} \dot{M}^{\frac{A-2B-1}{D}} M^{-\frac{A+2B+1}{2D}} R^{\frac{3(A+2B+1)}{2D}} \left(1 - \sqrt{\frac{R_\star}{R}}\right)^{\frac{A-2B-1}{D}} \tag{3.42}$$

  Where...

$$\Sigma_\star = \Sigma_0 \kappa_\star^{-2} \tag{3.43}$$

- The temperature profile of the disc is given by:

$$T = T_\star \alpha^{-\frac{2A}{D}} \dot{M}^{\frac{2(A+1)}{D}} M^{\frac{(2A+1)}{D}} R^{\frac{-3(2A+1)}{D}} \left(1 - \sqrt{\frac{R_\star}{R}}\right)^{\frac{2(A+1)}{D}} \tag{3.44}$$

  Where...

$$T_\star = T_0 \kappa_\star^2 \tag{3.45}$$

Where the opacity-independent constants (subscript 0) are defined as:

- $$H_0 = \frac{1.8}{16\pi c} \tag{3.46}$$
- $$\Sigma_0 = \frac{16^2 \pi c^2}{9.72\sqrt{G}} \tag{3.47}$$
- $$\rho_0 = \frac{16^3 \pi^2 c^3}{34.992\sqrt{G}} \tag{3.48}$$
- $$T_0 = \left(\frac{G\mu m_p}{2k_B}\right)\left(\frac{1.8}{16\pi c}\right)^2 \tag{3.49}$$

This class of models is appropriate if the results of [Brož et al., 2021] are correct and the ideal gas pressure and the radiation pressure are of similar magnitude in the disc. We present the results for the same opacities as for the $P_\mathrm{g} \gg P_\mathrm{r}$ class of models and additionally for $\kappa = 6 \cdot 10^{23} \rho^2 T^{-}1$.

3.3.3.1 Previously used opacity prescriptions

We first present results for the opacity approximations used for the $P_\mathrm{g} \gg P_\mathrm{r}$ case. The approximations are plotted in figs. 3.6 and 3.12. The latter approximation were found as fits of the 2D opacity function in the temperature range close to the kinematic model temperature profile.

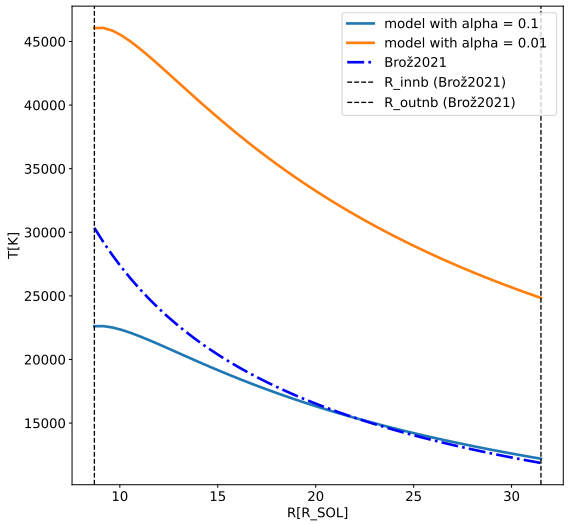

Figure 3.23: Temperature profile from the derived model ($P_g \approx P_r$, $\kappa = 6 \cdot 10^{24} \rho T^{-\frac{7}{2}}$) with parameters of the β Lyrae system and $\alpha = 10^{-1}, 10^{-2}$. Otherwise same as in fig.3.7.

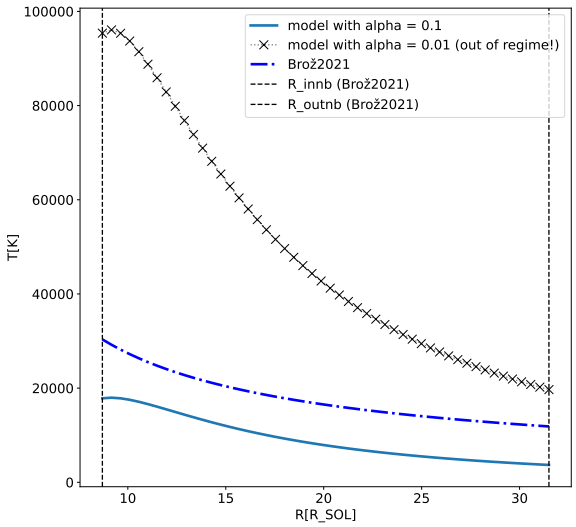

Figure 3.24: Temperature profile from the derived model ($P_g \approx P_r$, $\kappa = 10^{7.67}\rho^{0.72}T^{-0.1}$) with parameters of the β Lyrae system. Otherwise same as in fig. 3.7. The obtained profiles for $\alpha = 0.01$ aren't viable because it gives temperatures higher than the range in which the approximation of opacity plotted in fig. 3.12 holds.

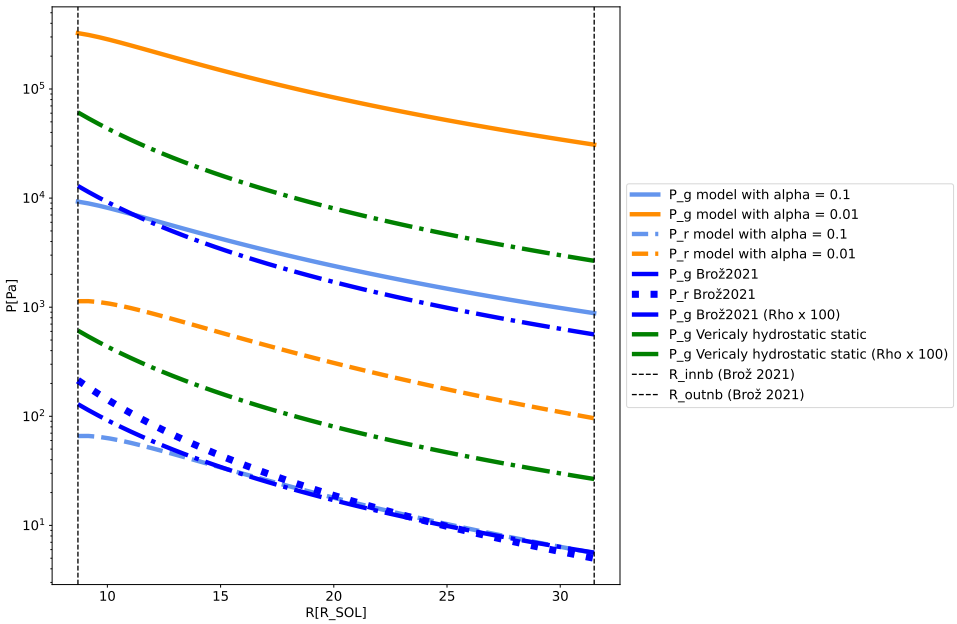

Figure 3.25: Ideal gas and radiation pressure profiles calculated for the derived model ($P_g \approx P_r$, $\kappa = 6 \cdot 10^{24}\rho T^{-\frac{7}{2}}$) with parameters of the β Lyrae system and $\alpha = 10^{-1}, 10^{-2}$. Otherwise same as in 3.10. The resulting profiles are not consistent with the $P_\mathrm{r} \approx P_\mathrm{g}$ assumption.

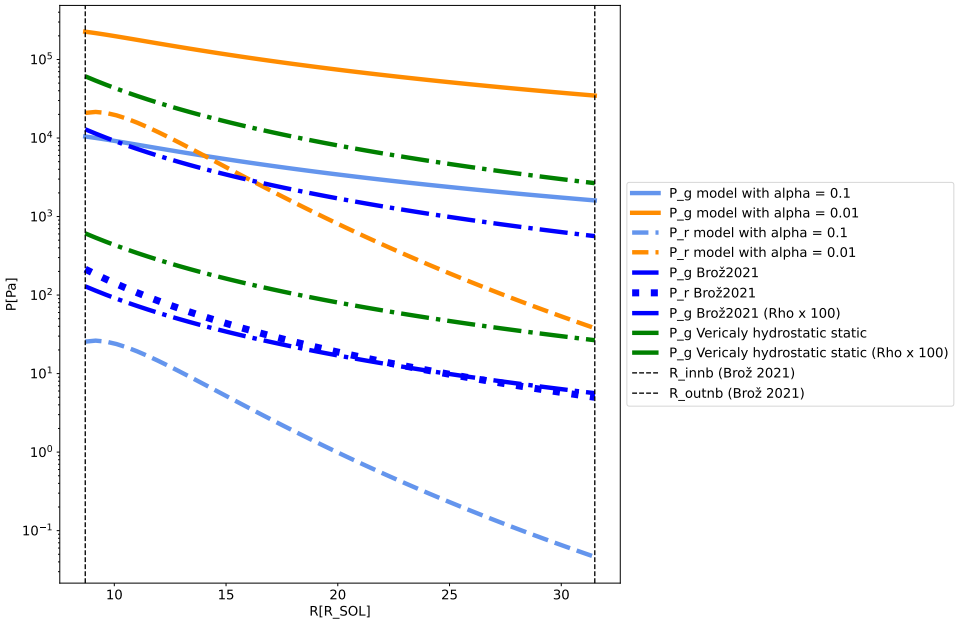

Figure 3.26: Ideal gas and radiation pressure profiles calculated for the derived model ($P_g \approx P_r$, $\kappa = 10^{7.67}\rho^{0.72}T^{-0.1}$) with parameters of the β Lyrae system and $\alpha = 10^{-1}, 10^{-2}$. Otherwise same as in 3.10. The resulting profiles are not consistent with the $P_\mathrm{r} \approx P_\mathrm{g}$ assumption.

Discussion of the $P_g \approx P_r$ models with previously used opacity prescriptions

- For $\kappa = \kappa_0\rho^{0.72}T^{-0.1}$ (3.24) profiles with $\alpha < 0.01$ must be considered false because the generated temperatures venture too far from the temperature range where the opacity approximations make sense.

- The temperature profile for Krammer's opacity with $\alpha = 0.1$ is in very good agreement with the kinematic model. The failures in the inner part of the disc may be attributed to stellar irradiation. $\kappa = \kappa_0\rho^{\frac{6}{10}}T^{-1.0}$ generated temperature profiles differ from the kinematic model too much in the observationally well-constrained outer part of the disc.

- In figures 3.25 and 3.26 we see that neither of the two models generate profiles consistent with the $P_\mathrm{g} \approx P_\mathrm{r}$ assumption, hence we must reject these models as false.

3.3.3.2 $P_\mathrm{g} \approx P_\mathrm{r}$ and an inverse problem for opacity

One can ask the inverse question; which opacity is necessary for $P_r = P_g$? We derived formulas for P_r and P_g with general constants A and B. $P_r = P_g$. Demanding that exponents of the same variable/parameter match lead to a set of four linear equations. Only two of them are linearly dependent, hence a unique solution cannot be obtained. So we searched for an opacity approximation that would ensure consistency with the $P_\mathrm{g} \approx P_\mathrm{r}$ at least in a part of the disc. The approximation shown in fig. 3.27 is what we found. We note that the approximation of the opacity is rather 'aggressively' adjusted to achieve the goal and does not correspond to Rogers and Iglesias [1992] very well.

$$\kappa = 6 \cdot 10^{23}\rho^2 T^{-1} \tag{3.50}$$

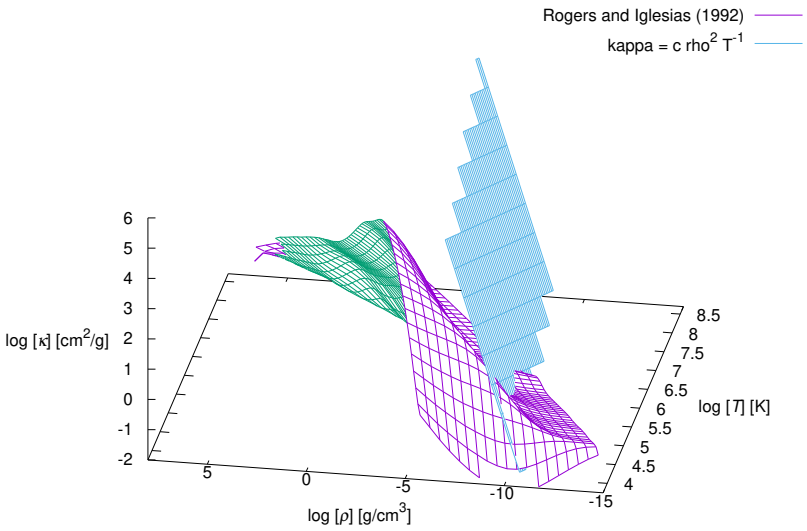

Figure 3.27: $\kappa = 6 \cdot 10^{23} \rho^2 T^{-1}$ surface. Otherwise same as in 3.6. This approximation corresponds to the inverse problem, not to the underlying opacity of Rogers and Iglesias [1992]. A tailored opacity to satisfy the $P_{\rm g} \approx P_{\rm r}$ at the output of the model in at least a part of the radial profile.

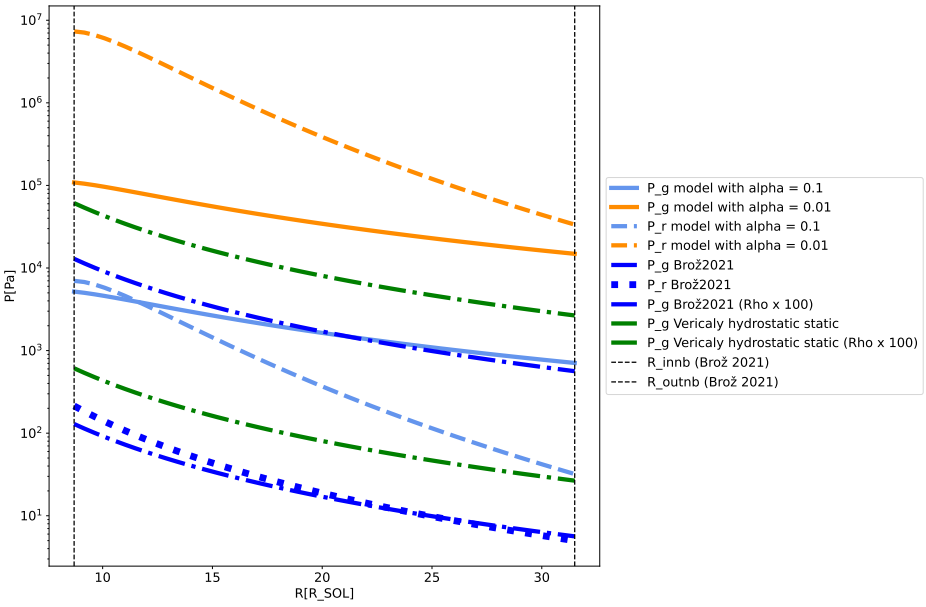

Figure 3.28: Ideal gas and radiation pressure profiles calculated for the derived model ($P_r \approx P_g$, $\kappa = 6 \cdot 10^{23} \rho^2 T^{-1}$) with parameters of the β Lyrae system and $\alpha = 10^{-1}, 10^{-2}$. See fig.3.10 for the description of the legend. The resulting profiles are consistent with the $P_g \approx P_r$ assumption only in the inner part of the disc.

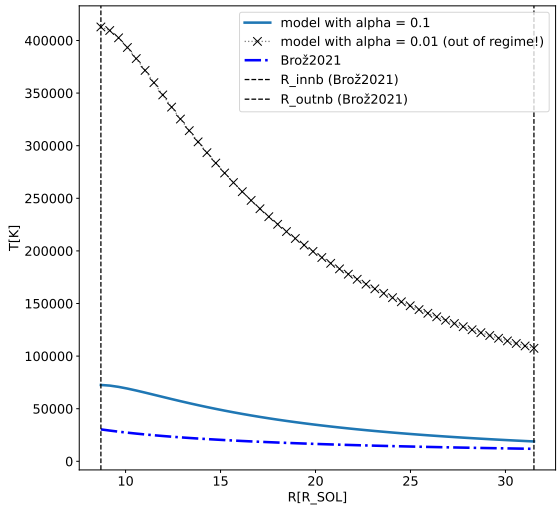

Figure 3.29: Temperature profile from the derived model ($P_r \approx P_g$, $\kappa = 6 \cdot 10^{23} \rho^2 T^{-1}$) with parameters of the β Lyrae system and $\alpha = 10^{-1}, 10^{-2}$. For a full description see fig. 3.7. The obtained profiles for $\alpha = 0.01$ aren't viable because it results in temperatures higher than the range in which the approximation of opacity holds (cf. fig. 3.27).

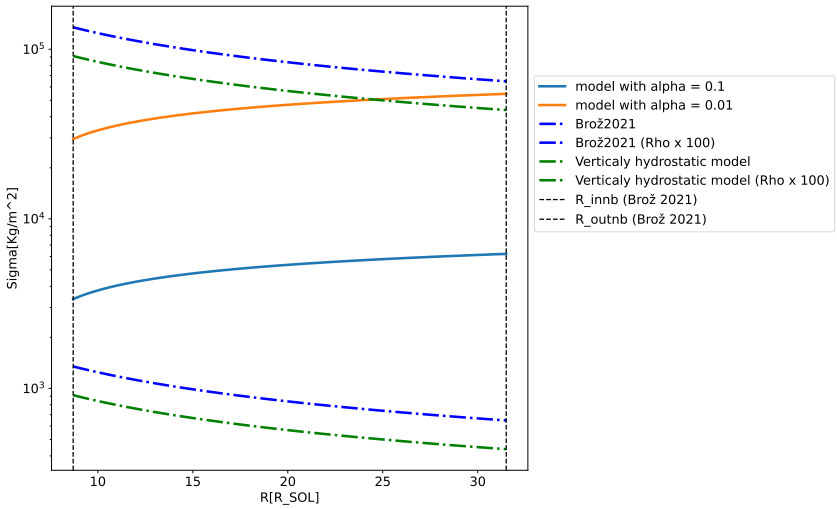

Figure 3.30: Vertically integrated density Σ profile from the derived model ($P_r \approx P_g$, $\kappa = 6 \cdot 10^{23} \rho^2 T^{-1}$) with parameters of the β Lyrae system. For full description see fig. 3.8. The analytical Σ -profiles are systematically larger than the fitted observations.

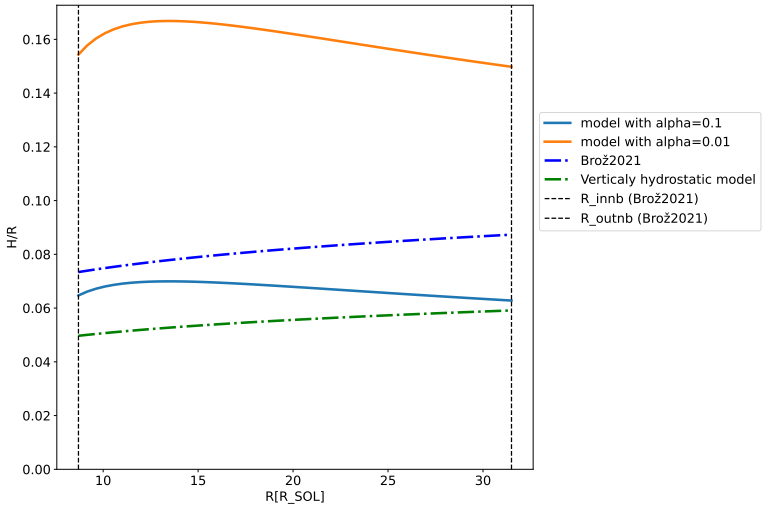

Figure 3.31: Aspect ratio profile from the derived model ($P_r \approx P_g$, $\kappa = 6 \cdot 10^{23}\rho^2 T^{-1}$) with parameters of the β Lyrae system.For a full description see fig. 3.10.

Discussion of the ($P_{\rm g} \approx P_{\rm r}$; $\kappa = 6 \cdot 10^{23}\rho^2 T^{-1}$) model

- For $\alpha = 0.1$ the model ensures consistency with the $P_g \approx P_r$ in the inner part of the disc (up to $15R_\odot$).
- For $\alpha > 0.1$ we must reject the model, the generated temperatures are too high from where the approximation makes sense (even this very bad approximation is more sensible for the region close to the temperature range of the kinematic model).
- The model with $\alpha = 0.1$ allows for almost a decent agreement with the kinematic model in the H/R ratio but requires a temperature that is double in the inner disc.

3.3.4 Models with $P_{\rm g} \ll P_{\rm r}$ assumed

For this class of models, we neglect the ideal gas pressure in the 3.17, and hence use;

$$P = \frac{4\sigma_B}{3c} T^4 \tag{3.51}$$

To obtain the temperature profile we calculate the energy density ϵ of radiation inside a layer according to [Shakura and Sunyaev, 1973];

$$\epsilon = \frac{9}{32\pi} \dot{M} \frac{GM_\star}{R^3} \frac{\kappa\Sigma}{c} \left(1 - \sqrt{\frac{R_\star}{R}}\right) \tag{3.52}$$

and use the Stefan-Boltzman law:

$$\epsilon = \frac{4\sigma_B}{c} T^4 \tag{3.53}$$

the resulting class of models is defined by the following equations:

- $$D = 12A + B + 4 \tag{3.54}$$
- Opacity profile in the disc is given by:

$$\kappa = \kappa_\star \alpha^{-\frac{4A+B}{D}} \dot{M}^{-\frac{8A}{D}} M^{\frac{B-4A}{2D}} R^{\frac{3(4A-B)}{2D}} \left(1 - \sqrt{\frac{R_\star}{R}}\right)^{-\frac{8A}{D}} \tag{3.55}$$

Where...

$$\kappa_\star = \left(\kappa_0 \rho_0^A T_0^B\right)^{\frac{4}{D}} \tag{3.56}$$

- The pressure scale height in the disc is given by:

$$H = H_\star \alpha^{-\frac{4A+B}{D}} \dot{M}^{\frac{D-8A}{D}} M^{\frac{(B-4A)}{2D}} R^{\frac{3(4A-B)}{2D}} \left(1 - \sqrt{\frac{R_\star}{R}}\right)^{\frac{D-8A}{D}} \tag{3.57}$$

Where...

$$H_\star = H_0 \kappa_\star \tag{3.58}$$

- The vertically integrated density in the disc is given by:

$$\Sigma = \Sigma_\star \alpha^{\frac{8A+2B-D}{D}} \dot{M}^{\frac{16A-D}{D}} M^{\frac{8A-2B-D}{2D}} R^{\frac{3(2B-8A+D)}{2D}} \left(1 - \sqrt{\frac{R_\star}{R}}\right)^{\frac{16-D}{D}} \tag{3.59}$$

Where...

$$\Sigma_\star = \Sigma_0 \kappa_\star^{-2} \tag{3.60}$$

- The temperature profile of the disc given by:

$$T = T_\star \alpha^{\frac{4A+B-D}{4D}} \dot{M}^{\frac{2A}{D}} M^{\frac{4A-B+D}{8D}} R^{\frac{3(B-4A-D)}{8D}} \left(1 - \sqrt{\frac{R_\star}{R}}\right)^{\frac{2A}{D}} \tag{3.61}$$

Where...

$$T_\star = T_0 \kappa_\star^{-\frac{1}{4}} \tag{3.62}$$

Where the opacity-independent constants (subscript 0) are defined as:

- $$H_0 = \frac{1.8}{32\pi c} \tag{3.63}$$

- $$\Sigma_0 = \frac{32^2 \pi c^2}{9.72\sqrt{G}} \tag{3.64}$$

- $$\rho_0 = \frac{32^3 \pi^2 c^3}{34.992\sqrt{G}} \tag{3.65}$$

- $$T_0 = \frac{72\sqrt{G} c^2}{9.72\sigma_B} \tag{3.66}$$

In sec. 3.2 we presented arguments against this class of models, yet it is still to be considered for the inner part of the disc where higher temperatures are possible, or in the case of considering alternative forms of energy transport in the vertical direction.

3.3.4.1 $P_g \ll P_r$; $\kappa = 10^{7.67}\rho^{0.72}T^{-0.1}$

As a first approach, we present the opacity approximation from fig. 3.12 that was presented also for the previous classes of models, let it serve for comparison.

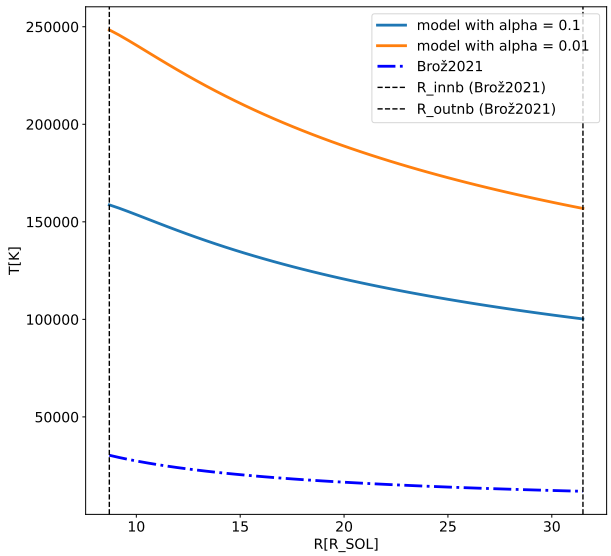

Figure 3.32: Temperature profile from the derived model ($P_g \ll P_r$; $\kappa = 10^{7.67}\rho^{0.72}T^{-0.1}$) with parameters of the β Lyrae system and $\alpha = 10^{-1}, 10^{-2}$ is compared to the temperature profile obtained by [Brož et al., 2021]. The obtained profiles for both studied α parameters aren't viable because they give temperatures higher than the range in which the approximation of opacity plotted in 3.12 holds.

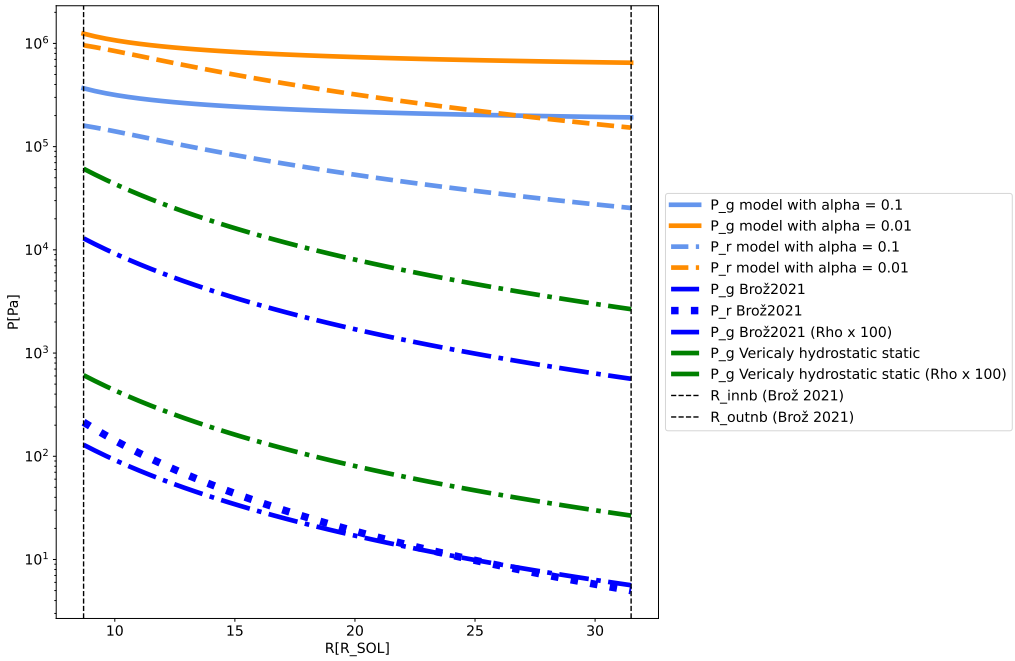

Figure 3.33: Ideal gas and radiation pressure profiles calculated for the analytical model ($P_g \ll P_r$; $\kappa = 10^{7.67}\rho^{0.72}T^{-0.1}$) with parameters of the β Lyrae system and $\alpha = 10^{-1}, 10^{-2}$. For a full description see fig. 3.10 The resulting profiles are not consistent with the $P_r \gg P_g$ assumption.

Discussion of the ($P_g \ll P_r$; $\kappa = 10^{7.67}\rho^{0.72}T^{-0.1}$) model.

- Both the pressure profiles in fig. 3.33 and temperature profiles in fig. 3.32 indicate we should reject this model, in the case of the studied system. The temperature profiles reach temperatures far outside the region where the opacity approximation is valid. The resulting pressure profile isn't consistent with the $P_{\mathrm{r}} \gg P_{\mathrm{g}}$ assumption.

- Generally, the radiation-pressure-dominated class of models generate higher temperatures compared to other classes. This is consistent with the $P_{\mathrm{r}} \propto T^4$ dependence.

3.3.4.2 $P_g \ll P_r$; $\kappa = 6 \cdot 10^{23}\rho^{0.5}T^{-3.5}$

Following the intuition that radiation pressure-dominated models should be valid for hotter discs, we searched for an opacity approximation in the $T \approx 10^5, 10^{5.5}$ K region (black hole accretion discs have temperatures of the order of 10^6K so we want to stay below that). This model is the result of these considerations. The opacity approximation is plotted in fig. 3.34:

$$\kappa = 6 \cdot 10^{23}\rho^{0.5}T^{-3.5} \tag{3.67}$$

The generated profiles are plotted in figs. 3.35, 3.36, 3.37 and 3.38.

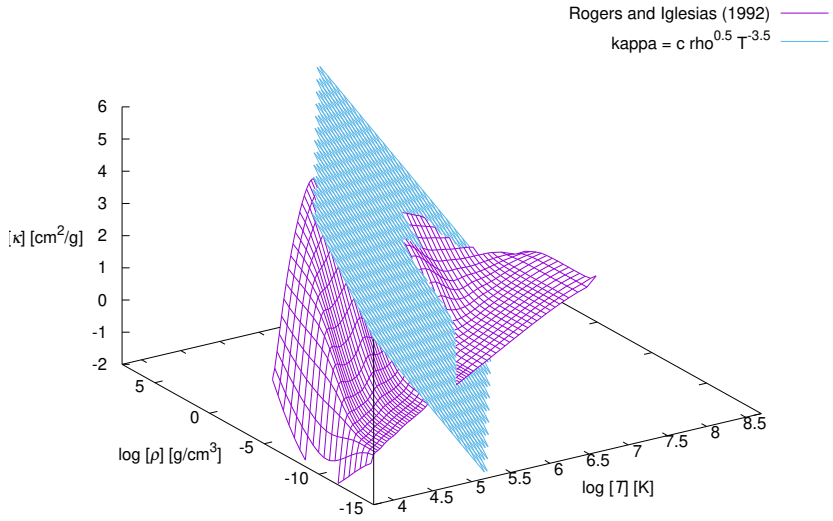

Figure 3.34: $\kappa = 6 \cdot 10^{23}\rho^2T^{-1}$ surface. Otherwise same as in fig. 3.6.The approximation was chosen as an inspection of opacity regimes that hold for higher temperatures.

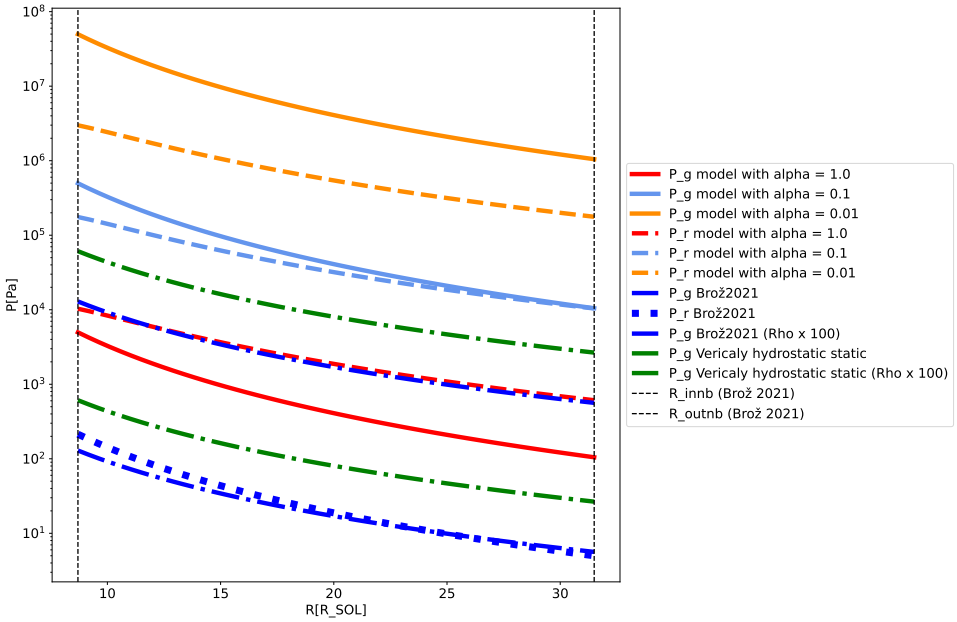

Figure 3.35: Ideal gas and radiation pressure profiles calculated for the derived model ($P_{\mathrm{r}} \gg P_{\mathrm{g}}$, $\kappa = 6{\cdot}10^{23}\rho^2 T^{-1}$) with parameters of the β Lyrae system and $\alpha = 1.0, 10^{-1}, 10^{-2}$. Otherwise same description as 3.10. The resulting profiles are only consistent with the $P_g \gg P_r$ assumption for α close to 1.0.

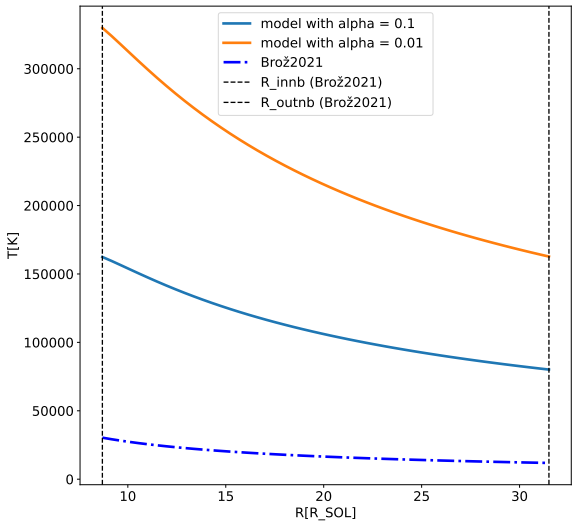

Figure 3.36: Temperature profile from the derived model ($P_{\mathrm{r}} \gg P_{\mathrm{g}}$, $\kappa = 6 \cdot 10^{23}\rho^2 T^{-1}$) with parameters of the β Lyrae system and $\alpha = 10^{-1}, 10^{-2}$ is compared to the temperature profile obtained by [Brož et al., 2021] The resulting temperatures are much higher than for models with other assumptions.

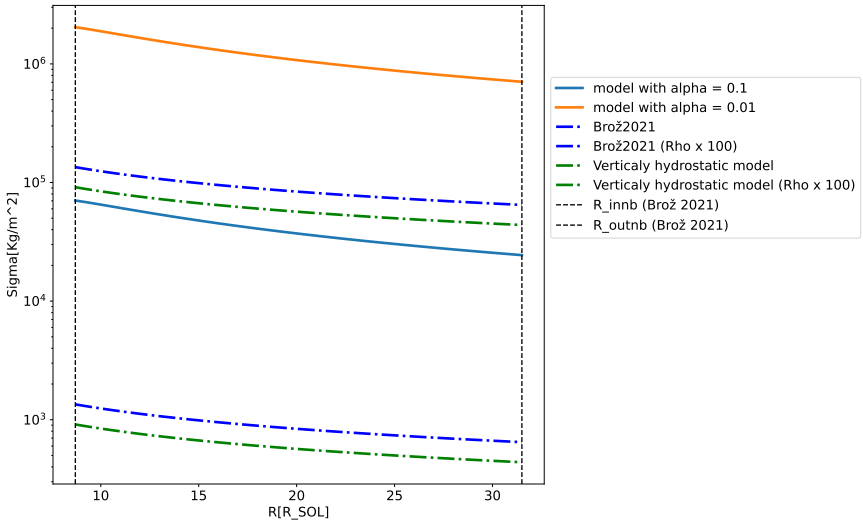

Figure 3.37: Vertically integrated density Σ profile from the derived model ($P_{\rm r} \gg P_{\rm g}$, $\kappa = 6 \cdot 10^{23} \rho^2 T^{-1}$) with parameters of the β Lyrae system and $\alpha = 10^{-1}, 10^{-2}$. Otherwise, see the description of fig. 3.8. The derived Σ-profiles are systematically larger than the fitted observations.

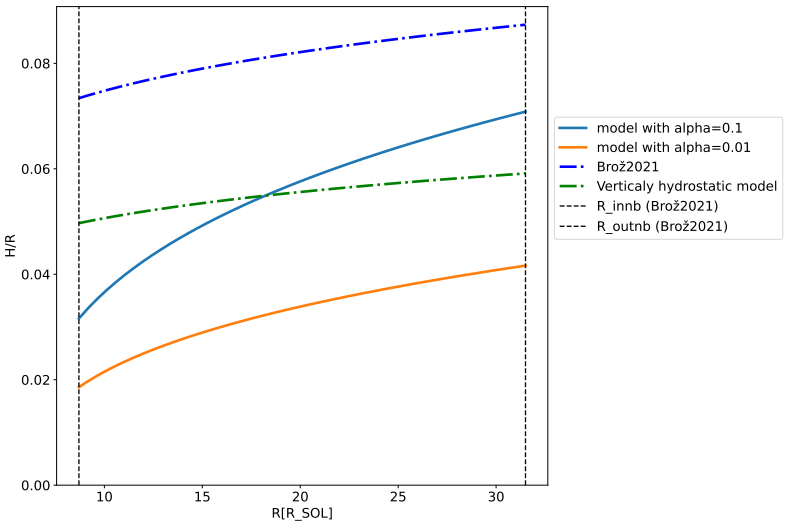

Figure 3.38: Aspect ratio profile from the derived model ($P_{\rm r} \gg P_{\rm g}$, $\kappa = 6 \cdot 10^{23} \rho^2 T^{-1}$) with parameters of the β Lyrae system. Otherwise, see the description of fig. 3.10. The radial dependency of the aspect ratio is much steeper than for other models.

Discussion of the($P_g \ll P_r$; $\kappa = 6 \cdot 10^{23} \rho^{0.5} T^{-3.5}$) model.

- From the pressure profiles in fig. 3.35 we see that the $P_g \ll P_r$ is satisfied for α close to 1.0.
- Higher temperature discs (lower α) seem to produce a thinner disc, which is contra-intuitive. Here we note that this aspect of the model should not necessarily be taken to be real, since it is for cases that are not consistent with the $P_{\rm g} \ll P_{\rm r}$ assumption and around $\alpha \approx 1.0$, where the assumption is met, the effect is very weak; $T \propto \alpha^{0.3}$.
- If we take the predictions of Σ and H from the other models as correct ones, then it seems possible to construct a much hotter disc with a similar vertical extent and similar Σ.